Microporous and Mesoporous Materials 173 (2013) 86–91

Contents lists available at SciVerse ScienceDirect

Microporous and Mesoporous Materials

journal homepage: www.elsevier.com/locate/micromeso

MOF stability and gas adsorption as a function of exposure to water, humid air, SO_2, and NO_2

Sangil Han, Yougui Huang, Taku Watanabe, Sankar Nair, Krista S. Walton, David S. Sholl, J. Carson Meredith *

School of Chemical & Biomolecular Engineering, Georgia Tech, Atlanta, GA 30332-0100, USA

ARTICLE INFO

Article history:
Received 10 September 2012
Received in revised form 5 December 2012
Accepted 6 February 2013
Available online 16 February 2013

Keywords:
Metal organic frameworks
Carbon capture
Separation
High-throughput
Acid gas

ABSTRACT

Gas adsorption and stability to liquid water, humid air, and acid gasses on metal organic frameworks have been studied using a high-throughput adsorption measurement system. Among the seven MOFs studied, Cu-HF, Zn-NDC, and Ni-NIC showed higher CO_2/N_2 sorption selectivities, (8–12), than the other MOFs (~4), mainly due to high CO_2 adsorption. Long term (5 days) NO_2 exposure, as well as exposure to liquid water, resulted in partial decomposition of the original structure of Zn-NDC with a corresponding 26–30% decrease in CO_2 adsorption capacity. No noticeable changes in X-ray diffraction (XRD) patterns were observed for the other MOFs with small variations in adsorption capacities, indicating structural robustness to acid gas and liquid water. Short-term exposure to humid air (3 d) and acid gasses (2 d) caused a decrease in CO_2 and N_2 adsorption capacity for Cu-HF and an increase in adsorption capacity for Ni-NIC. Measurements indicate that pore flexibility in Cu-HF, Zn-NDC, Ni-NIC and Cu-NH_2 is modulated by temperature: large SF_6 molecules are rejected from the pores at room temperature (as expected based on kinetic diameter), but N_2, which does adsorb internally at room temperature, is rejected from the pores at 77 K.

1. Introduction

The capture of CO_2 from fossil fuel combustion flue gas is the focus of significant research efforts in response to concern over the role of CO_2 in climate change. A significant fraction of CO_2 emissions comes from the burning of oil, coal, and natural gas [1]. Current technologies for capturing CO_2 from these sources are largely based on chemical absorption of CO_2 by amine solutions, but these suffer from a high energy penalty due to the high-temperature regeneration of the sorbent [2]. Furthermore, the regeneration process can cause sorbent loss and degradation [3]. Hence, there is a critical need to discover and develop more energy efficient and sustainable capture technologies [4].

Metal organic frameworks (MOFs) are one class of materials that has received considerable attention as possible components in CO_2 capture technologies [5]. MOFs are nanoporous materials with high surface area and well-defined pore structure that have potential applications in separation, catalysis, and gas storage [6,7]. There are an enormous number of MOFs that can be synthesized with various combinations of organic linkers and metal centers, providing an opportunity to tailor surface area, pore size, and surface functionality [8]. MOFs have been considered for use in CO_2 capture both as sorbents [9–13] and as components in membranes [14–16].

For practical CO_2 capture applications, the performance of MOFs that have been exposed to water vapor and acid gasses like SO_2 and NO_2 is critical, since these are ubiquitous components of post-combustion flue gas. However, to date there have been relatively few studies of MOF stability with respect to water [17–20] and, to our knowledge, there are a few studies of stability with respect to acid gasses [19,21,22]. In this study, we present adsorption properties of CO_2 and N_2 for seven MOFs by using a high-throughput (HT) sorption system described previously [19]. Additionally, the structural stability and dependence of adsorption and selectivity following exposure to humid air, liquid water, and acid gasses were investigated. The potential role of structural flexibility of the MOF frameworks on gas adsorption was examined by measuring SF_6 adsorption. Our results considerably extend the number of MOFs for which information on stability with respect to acid gasses is available, and demonstrates the value of the relatively inexpensive experimental methods we have developed to achieve this goal.

2. Experimental

2.1. Materials

Eight MOFs were synthesized for this study following the synthesis procedures from previous literature: $\{CdZrSr(C_2O_4)_4{\cdot}6H_2O\}_n$

* Corresponding author. Address: School of Chemical & Biomolecular Engineering, Georgia Institute of Technology, 311 Ferst Drive, Atlanta, GA 30332-0100, USA. Tel.: +1 404 385 2151; fax: +1 404 894 2866.
E-mail address: carson.meredith@chbe.gatech.edu (J. Carson Meredith).

1387-1811/$ - see front matter © 2013 Elsevier Inc. All rights reserved.
http://dx.doi.org/10.1016/j.micromeso.2013.02.002

Table 1
Reference code, largest cavity diameter (LCD), pore limiting diameter (PLD), and surface area predicted by theory and measured by N_2 physisorption at 77 K. The CuHF results are from sample CuHF1.

	REFCODE	LCD, Å	PLD, Å	Theoretical surface area, m^2/g	Experimental surface area, m^2/g
CdZrSr	BEVQID	2.752	2.314	618	4.52
Ni-Nic	VOCNOQ	4.367	3.225	117	0
La-Cu	XOHJUA	3.484	2.951	509	2.08
Eu-Cu	DOHYIJ	3.615	3.055	548	5.74
Zn-NDC	JASNEX	3.183	2.608	902	53.6
$ZnPO_3$	OFIWIK	4.18	3.15	223	0
Cu-HF	ESIPUR	4.847	2.732	545	12

(denoted CdZrSr below) [23], $\{[Ni_2(NIC)_4(\mu H_2O)]\cdot CH_3CH_2OH\cdot H_2O\}_n$ (Ni-NIC) [24], $\{[LnCu(nic)_2(C_2O_4)]\cdot xH_2O\}_n$ (La-Cu) [25], $\{[EuCu(NIC)_2(C_2O_4)]\cdot xH_2O\}_n$ (Eu-Cu) [26], $\{[Zn_2(2,6\text{-ndc})_2(bpy)]\}_n$ (Zn-NDC) [27], $\{(C_6H_{14}N)_2[Zn_3(HPO_3)_4]\}_n$ ($ZnPO_3$) [28], and $\{Cu(hfipbb)(H_2hfipbb)_{0.5}\}_n$ (Cu-HF) [29]. Details of the synthesis conditions for these materials are given in Supporting Information. The identity of each material was confirmed using powder X-ray Diffraction (PXRD) experiments. These MOFs were selected based on computational screening of a large number of previously reported MOFs using geometric characterization of the MOFs' pore structures [16,30]. The MOFs were chosen to have pore limiting diameters (PLD) similar to or smaller than the nominal kinetic diameter of CO_2 and N_2 in order to consider materials that can potentially have both adsorption and diffusion selectivity favoring CO_2 over N_2. MOFs with pores that are large relative to the size of adsorbed molecules are typically not expected to have any diffusion selectivity for CO_2 relative to N_2 [31]. Table 1 lists the PLD and also the largest cavity diameter (LCD) for each material calculated using the methods of Haldoupis et al. [30] based on the assumption that the reported crystal structure for each material is rigid.

An important issue when using small-pore MOFs is whether molecules of interest can penetrate into the pores of the MOF. A standard characterization of this issue is to calculate surface area from the Brunauer–Emmett–Teller (BET) model applied to N_2 physisorption measurements at 77 K. The BET surface areas for each MOF, measured after activation at 180–200 °C for 20 h under vacuum, are listed in Table 1. Although the theoretically predicted surface areas from the MOF crystal structures range from 116 to 902 m^2/g, most of the materials showed negligible experimental adsorption of N_2 at 77 K. We show below with room temperature N_2 adsorption data and additional experiments using adsorption of SF_6 that these observations result from limitations in kinetics at the low temperature employed. That is, these MOFs have internal surface area that is suitable for N_2 adsorption, but at 77 K the kinetics of N_2 adsorption are so slow that they yield low apparent surface areas in our experiments. This phenomenon has been reported previously for small pore MOFs [19,32,33].

2.2. Adsorption measurements

The adsorption amounts of the MOFs were measured by using a HT sorption system described previously [19]. The instrument enables measurement of gas adsorptio[31]n by monitoring pressure decay as a function of time in parallel for up to 36 samples following exposure to pure gasses at 1 atm and 30 °C. The final equilibrium pressure in each chamber depends on the adsorption loading of the material being examined, so care must be taken to describe measurements in terms of this final pressure, not the uniform initial pressure. In our previous report, calibration experiments that confirmed the precision of this technique were described [19]. An initial sample size of approximately 50 mg of each MOF was used. The MOFs were activated at 160–280 °C for 17 h under vacuum prior to measurements (Table S1 in Supporting Information). Between the measurements, samples were degassed for 5 h under 0.02 atm vacuum at room temperature. The measurements were repeated in triplicate. Two different samples of Cu-HF were used, which differed in their activation temperatures. The sample denoted Cu-HF1 (Cu-HF2) below was activated at 280 °C (190 °C).

2.3. Stability tests

To provide information on the stability of each MOF with respect to water and acid gasses, gas adsorption (with dry, single component gasses) was measured before and after exposure of MOF samples to humidity and, separately, acid gasses in humid air. In each case, the MOFs were evacuated at 130 °C under vacuum for 20 h after the exposure prior to the adsorption measurements. In real applications it is of course vital that materials for CO_2 capture perform effectively during exposure to humidity and acid gasses. Although our protocol does not probe this situation, any material that is not stable after the staged exposure in our experiments should certainly be rejected from consideration from further development. In this way, our approach defines an efficient means to make go/no-go decisions regarding the viability of individual MOFs for CO_2 capture applications.

Samples were exposed to air with relative humidity of 80% for 3 days at room temperature. To test MOFs with acid gasses, the

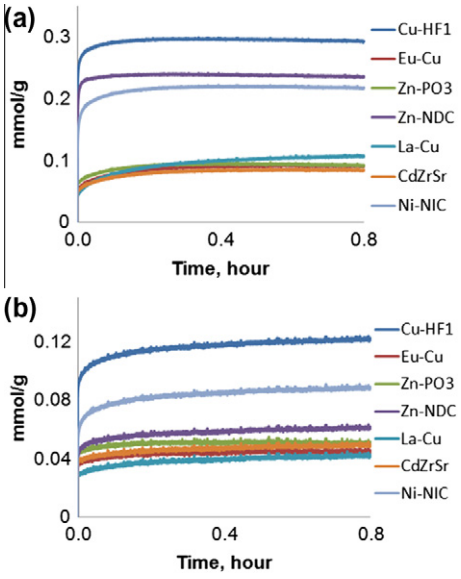

Fig. 1. Adsorption kinetics of the MOFs with initial pressure of 14 psi at 30 °C. (a) CO_2, (b) N_2.

Table 2
Equilibrium pressures measured at 30 °C. Results for Cu-HF are from sample Cu-HF1.

	Before water vapor, atm		After water vapor, atm		After SO_2 for 2 d and NO_2 for 2 d, atm	
	CO_2	N_2	CO_2	N_2	CO_2	N_2
Cu-HF	0.197	0.660	0.245	0.714	0.272	0.714
Eu-Cu	0.592	0.776	0.578	0.776	0.531	0.769
$ZnPO_3$	0.653	0.803	0.653	0.789	0.660	0.776
Zn-NDC	0.354	0.796	0.333	0.782	0.347	0.776
La-Cu	0.680	0.844	0.687	0.844	0.660	0.837
CdZrSr	0.633	0.776	0.612	0.769	0.619	0.755
Ni-Nic	0.238	0.667	0.156	0.626	0.095	0.605

MOFs were exposed to 15 ppm of SO_2 for 2 days (short-term) or 5 days (long-term) and then 15 ppm of NO_2 for 2 days or 5 days in humid air (80% relative humidity) at 27 °C. These gas mixtures were prepared using salt solutions according to the literature [34]. The 15 ppm of SO_2 gas was generated with a 500 μg/ml $NaHSO_3$ aqueous solution with pH 3.7 at 45 °C. 200 ml/min of air flow transferred the generated SO_2 gas from reaction tube into a desiccator which has 80% relative humidity prepared with a saturated NaCl solution. The 10 ppm of NO_2 gas was generated by using the same apparatus under different conditions (800 μg/ml of $NaNO_2$ aqueous solution with pH 3 at 45 °C with 100 ml/min of air flow). Gas concentrations were verified with Dräger-Tubes (Dräger, Germany).

We also investigated the stability of MOFs with respect to liquid water. Deionized water was dropped onto each MOF in the sample chamber of the HT sorption system and then MOFs were left for 2 days at room temperature. The MOF samples were evacuated at 130 °C under vacuum for 20 h after the exposure prior to the adsorption measurements.

3. Results and discussion

Fig. 1 shows the adsorption kinetics for each MOF for CO_2 (Fig. 1a) and N_2 (Fig. 1b) prior to the exposure of the MOFs to humid air or acid gasses. Adsorption was measured at 30 °C. The equilibrium loading was averaged over 0.4–0.8 h for CO_2 and 0.6–0.8 h for N_2, where trendline slopes for the adsorption curves remain below 0.008. The material-dependent equilibrium (final) pressures for these measurements ranged from 0.20 to 0.68 atm for CO_2 and 0.61 to 0.82 atm for N_2. As stated above, the final pressure in each experiment is dependent on the adsorption loading of the material being tested. The specific equilibrium pressures for each

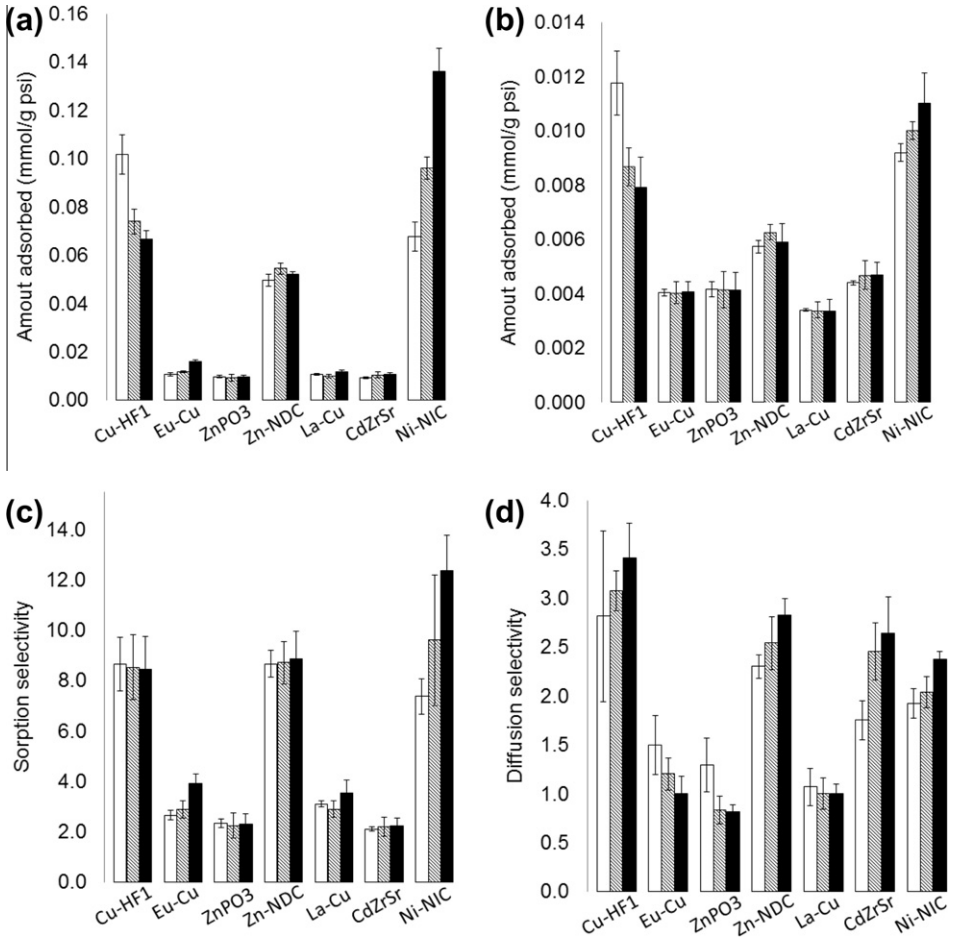

Fig. 2. (a) CO_2 and N_2, (b) adsorption capacities and sorption, (c) diffusion and (d) selectivities measured at 30 °C. White (before humid air), gray (after humid air for 3 d), and black (after SO_2-humid air exposure for 2 d and NO_2-humid air exposure for 2 d). Error bars represent standard deviation (n = 3).

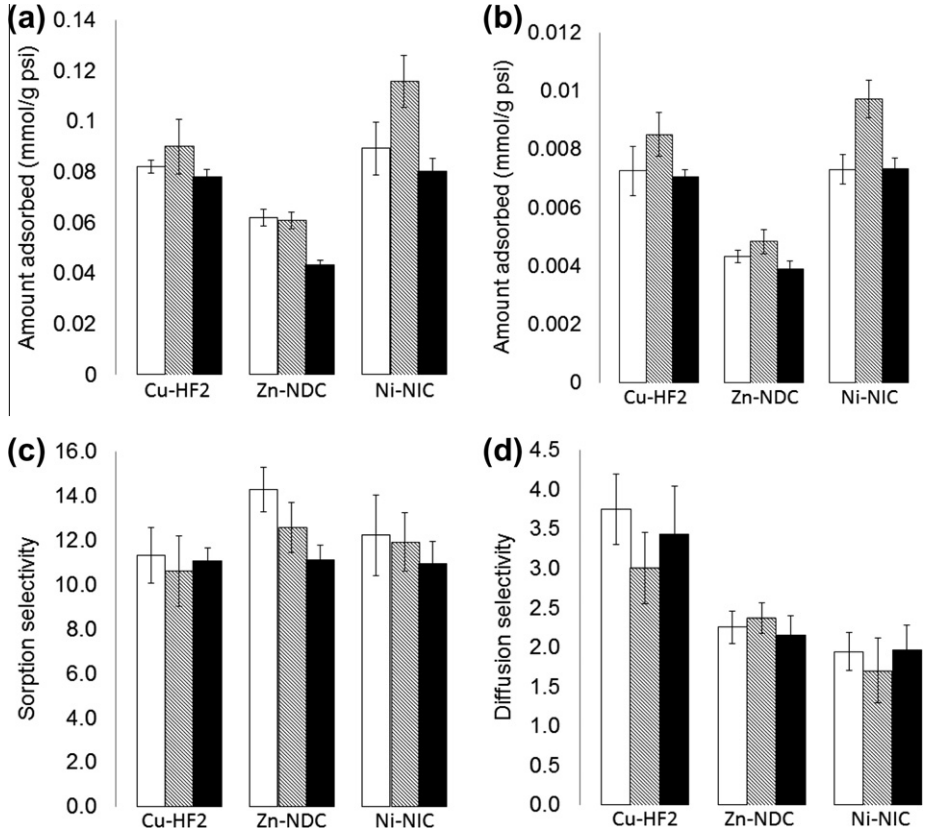

Fig. 3. (a) CO_2 and N_2, (b) adsorption capacities and sorption, (c) diffusion and (d) selectivities measured at 30 °C after long-term exposure to acid gasses. White (before exposure), gray (after SO_2-humid air exposure for 5 d), black (after NO_2-humid air exposure for 5 d). Error bars represent standard deviation ($n = 3$).

Table 3
Adsorption capacity before and after long-term (5 d) SO_2 and NO_2 exposure and liquid water exposure. Results for Cu-HF are from sample Cu-HF1. Δ was calculated on the basis of the adsorption capacities measured before exposure.

	No exposure, mmol/g psi		After SO_2 for 5 days		After NO_2 for 5 days		After liquid water for 2 days	
	CO_2	N_2	$\Delta_{CO2,}$ %	$\Delta_{N2,}$ %	$\Delta_{CO2,}$ %	$\Delta_{N2,}$ %	$\Delta_{CO2,}$ %	$\Delta_{N2,}$ %
Cu-HF	0.082	0.0073	9.6	17.1	−5.0	−2.9	15.4	9.2
Ni-Nic	0.089	0.0073	29.7	33.0	−10.1	0.4	−2.5	−7.6
Zn-NDC	0.062	0.0043	−2.0	11.5	−30.1	−10.0	−26.5	−8.3

MOF are reported in Table 2. Fig. 2a and b show adsorption capacities for CO_2 and N_2, respectively, obtained from the average adsorption values after reaching the final pressure in each experiment. To compare the adsorption measurements among different materials, the adsorbed amounts are normalized by dividing by the equilibrium pressure. Fig. 2c reports the adsorption selectivity as the ratio of the CO_2 and N_2 normalized adsorbed amounts. Cu-HF, Zn-NDC, and Ni-NIC showed relatively high CO_2 and N_2 adsorption compared to the other MOFs.

Fig. 2 also shows the adsorption loading of CO_2 and N_2 after each sample had been exposed to humid air (3 days) and, separately, to acid gasses in the presence of humidity for 2 days each. There were no significant changes in adsorption loading after exposure to humid air and to acid gasses except for Cu-HF and Ni-NIC. The adsorbed amounts for both gasses decreased for Cu-HF and increased for Ni-NIC after exposure to humid air and acid gasses. From Fig. 2c, adsorption selectivities were ~8 for Cu-HF and Zn-NDC and ranged from 8 to 12 for Ni-NIC, similar to the range observed for ZIF-90, ZIF-8, ZIF-7, and Zn-TTC in our previous study [19]. Relatively low adsorption selectivities, ~4, were observed for Eu-Cu, $ZnPO_3$, La-Cu, and CdZrSr. With the exception of Eu-Cu and Ni-NIC, the adsorption selectivity was insensitive to exposure to humidity and acid gasses. Eu-Cu and Ni-NIC showed increased selectivity following humid air and acid gas exposure. Small changes in PXRD patterns were observed for some of the MOFs: reduced intensity at 9°, 18°, and 21° for Zn-NDC; reduced intensity at 6° and 7° and increased intensity at 17° for $ZnPO_3$; width changes at 13°, 23°, and 32° for CdZrSr; peak disappearance at 8° and increased intensity at 13° and 15° for Cu-HF; increased intensity at 12°, 30°, and 42° for Eu-Cu. However, no changes in PXRD patterns were observed for Ni-NIC and La-Cu after humid air and acid gas exposure (Fig. S1 in Supporting Information), indicating that the humid air and acid gasses had little or no effects on crystal structure.

Diffusion selectivities for the MOFs were estimated by using a micropore diffusion model (Eq. (1)) [35] assuming that mass transfer resistance in our experiments was dominated by intracrystalline diffusion:

$$1 - \frac{m_t}{m_\infty} \approx \frac{6}{\pi^2} \exp\left(\frac{-\pi^2 D_c t}{r_c^2}\right) \quad (1)$$

where D_c is intracrystalline diffusity, (m_t/m_∞) is fractional uptake, r_c is particle radius and t is time. The adsorption kinetics where the

adsorbed amounts are between 70% and 90% of the equilibrium loading were used to estimate diffusivities in each sample. This late kinetic regime was chosen in order to mitigate the fact that Eq. (1) assumes a constant gas phase concentration (a condition that is not technically met by our experiment), since concentration changes more slowly towards the end of the transient regime. The diffusion selectivity is taken to be the ratio of the single component diffusion coefficients. The diffusion selectivities were 2 to 3.5 for Cu-HF, Zn-NDC, CdZrSr, and Ni-NIC. In large pore materials where diffusion can be approximated by Knudsen diffusion, N_2 would diffuse faster than CO_2, leading to a diffusion selectivity of ~0.8. Eu-Cu, $ZnPO_3$, and La-Cu showed almost no diffusion selectivity for CO_2 relative to N_2 around 1 (Fig. 2d). The observed diffusion selectivity for $ZnPO_3$ and CdZrSr was more sensitive to exposure to humidity and acid gasses than the adsorption selectivity was for the same materials. An important caveat for interpreting these diffusion results is that our data does not allow us to verify the assumption that intracrystalline diffusion dominates mass transport in each sample chamber. A more thorough examination of this issue would require experiments with particles of multiple sizes for each material, a step that is beyond the scope of this work.

We further examined longer-term stability after 5 day exposures to SO_2 and NO_2 gas exposure for the Zn-NDC, Cu-HF, and Ni-NIC, which showed higher sorption selectivities than other MOFs. These MOFs were exposed to 10 ppm SO_2 for 5 days, and then exposed to 10 ppm NO_2 for 5 days under humid air with 80% relative humidity. The adsorption of CO_2 and N_2 was measured and XRD patterns were taken after exposure to each acid gas. In the 5 day stability test, an 18% lower CO_2 adsorption capacity prior to exposure to humidity (0.082 mmol/g psi) was observed for sample Cu-HF2 than that measured in the short-term stability test (0.1 mmol/g psi), which used sample Cu-HF1. We attribute this deviation to the difference in activation temperatures of the separate Cu-HF samples. The XRD patterns for Cu-HF1 and Cu-HF2 showed clear differences after activation at these two different temperatures (Figs. S1 and S2 in Supporting Information). Ni-NIC showed increased CO_2 and N_2 adsorption capacities after the long-term SO_2 exposure (Fig. 3 and Table 3), similar to the behavior observed after short-term SO_2 and NO_2 exposure (Fig. 2a and b). Adsorption and diffusion selectivities remained constant after the long-term acid gas exposure for all MOFs except Zn-NDC. The CO_2 adsorption decrease of 30% for Zn-NDC resulted in a decrease of adsorption selectivity from 14.3 to 11.1 after the long-term NO_2 exposure. Partial decomposition of the original structure in Zn-NDC was confirmed by PXRD patterns which showed peak disappearance and reduced peak intensity after the long-term NO_2 exposure with humid air for 5 days (Fig. S2 in Supporting Information). There were no noticeable changes in PXRD patterns for Ni-NIC and Cu-HF after long-term exposure.

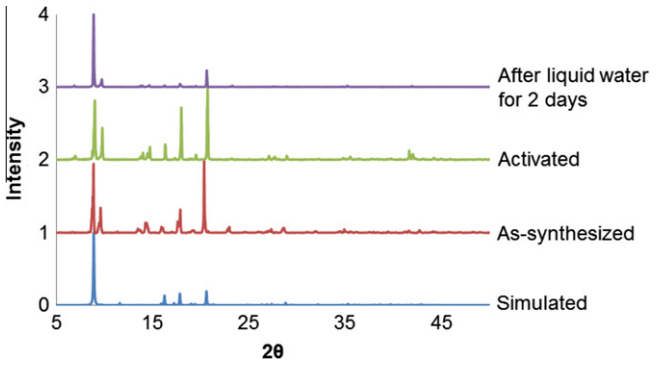

Fig. 4. XRD patterns of Zn-NDC before and after liquid water exposure for 2 d at 25 °C.

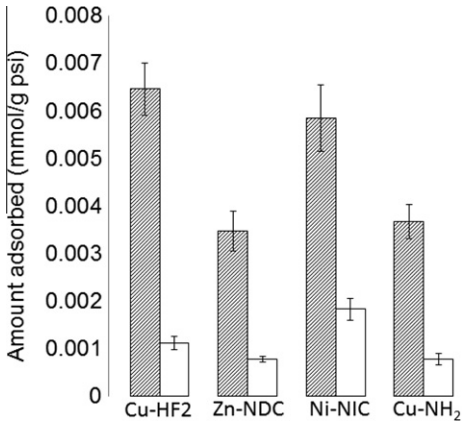

Fig. 5. N_2 (gray) and SF6 (white) adsorption capacities measured at 30 °C. Error bars represent standard deviation (n = 3).

In practical applications involving flue gas, water adsorption could affect the performance of adsorbents. Thus, we investigated the stability and adsorption performance for Cu-HF, Ni-Nic, and Zn-NDC after exposure to liquid water. Adsorption capacities were measured and PXRD patterns were taken before and after exposure to liquid water for 2 days at room temperature. Ni-NIC and Cu-HF were stable with respect to liquid water exposure, giving similar adsorption capacities and PXRD patterns (Fig. S3 in Supporting Information) before and after the liquid water exposure. Zn-NDC, however, showed a decrease in CO_2 adsorption by 27% (Table 3) and significantly reduced peaks in XRD patterns at 9.8°, 13.7°, 14.5°, 16.3°, 17.9° and 21° (Fig. 4). While the water vapor exposure of Zn-NDC resulted in no decrease in adsorption capacities (Fig. 2), PXRD peak intensities were reduced at 9.6°, 17.8° and 21° after the exposure to humid air (Fig. S1).

As we showed above, most of the materials we have examined showed negligible BET surface area when characterized with N_2 adsorption at 77 K. The measurable loadings of N_2 at room temperature in these materials, however, suggest that N_2 is able to diffuse into the pores of these MOFs at non-cryogenic temperatures. To verify this observation, we used our adsorption apparatus to measure the adsorption of SF_6 at room temperature with Cu-HF, Zn-NDC, and Ni-NIC. This measurement was also performed using Cu-NH_2 ($\{Cu_4(NH_2)_4(Pyridine)_2(H_2O)_2\}_n$), another small pore MOF [36]. SF_6 is considerably larger and more polarizable than N_2, so it adsorbs far more readily than N_2 into pores that are accessible to both species [37]. The adsorption loading of SF_6 was considerably lower than for N_2 in all four MOFs (Fig. 5) Table 4. The small cavity diameters of the MOFs we have used and the small adsorbed amounts make it highly unlikely that any penetration of SF_6 into the MOF pores occurred. These results support the observation that N_2 can readily diffuse into these MOFs at room temperature, lending weight to the idea that internal pore flexibility must be accounted for in detailed molecular models of adsorbate diffusion in small pore materials [16,38]. They also indicate that the contri-

Table 4
Experimental adsorption and estimated external adsorption of SF_6 on four MOFs at 30 °C.

	LCD, Å	PLD, Å	Particle size[a], μm	Experimental adsorption, mmol/g psi	Estimated adsorption, mmol/g psi	Estimated/ experimental, %
Ni-Nic	4.37	3.23	20	0.00183	0.00060	33
Cu-HF	4.85	2.73	83	0.00112	0.00016	14
Zn-NDC	3.18	2.61	102	0.00077	0.00012	16
Cu-NH_2	4.13	2.62	30	0.00078	0.00043	55

[a] Particle size was estimated from SEM images (Fig. S4 in Supporting Information). Cu-NH2 was activated at 120 °C under vacuum for 5 h.

butions to the adsorption loadings of N_2 and CO_2 in our samples are small.

4. Conclusions

Seven MOFs were characterized to identify sorption and diffusion selectivities of CO_2/N_2 before and after exposure to humid air, acid gasses and liquid water. Adsorption selectivities for Cu-HF, Zn-NDC, and Ni-NIC were similar to those for ZIFs and Zn-TTC, however lower than Co-NIC and Cu-PCN. Short term humid air (3 d) and acid gas (2 d) exposures caused CO_2 and N_2 adsorption capacity to decrease for Cu-HF and to increase for Ni-NIC. Adsorption selectivity, on the other hand, was unchanged except for an increase observed after exposure to humid air and acid gas for Eu-Cu and Ni-NIC. In the long-term (5 d) acid gas exposure and the liquid water exposure, the original framework structures of Cu-HF and Ni-NIC remained stable with no decrease in adsorption capacity. However, according to the XRD patterns, Zn-NDC showed partial decomposition of the original framework concomitant with a decrease in CO_2 sorption capacity by 26–30%. The observation that N_2 can readily diffuse into these MOFs at room temperature lends credence to the idea that internal pore flexibility must be accounted for in detailed molecular models of adsorbate diffusion in small pore materials.

Acknowledgements

We gratefully acknowledge support from the DOE ARPA-E IMPACCT program under grant DE-AR0000074.

Appendix A. Supplementary data

Supplementary data associated with this article can be found, in the online version, at http://dx.doi.org/10.1016/j.micromeso.2013.02.002.

References

[1] J.-R. Li, Y. Mab, M.C. McCarthy, J. Sculleya, J. Yu, H.-K. Jeong, P.B. Balbuena, H.-C. Zhou, Coord. Chem. Rev. 255 (2011) 1791.
[2] K. Sumida, D.L. Rogow, J.A. Mason, T.M. McDonald, E.D. Bloch, Z.R. Herm, T.-H. Bae, J.R. Long, Chem. Rev. 122 (2012) 724–781.
[3] J. Tan, H. Shao, J. Xu, L. Du, G. Luo, Ind. Eng. Chem. Res. 50 (2011) 3966–3976.
[4] A. Samanta, A. Zhao, G.K.H. Shimizu, P. Sarkar, R. Gupta, Ind. Eng. Chem. Res. 51 (2012) 1438–1463.
[5] S. Keskin, ChemSusChem 3 (2010) 879.
[6] J.R. Long, O.M. Yaghi, Chem. Soc. Rev. 38 (2009) 1213–1214.
[7] S.T. Meek, J.A. Greathouse, M.D. Allendorf, Adv. Mater. 23 (2011) 249–267.
[8] C.E. Wilmer, M. Leaf, C.Y. Lee, O.K. Farha, B.G. Hauser, J.T. Hupp, R.Q. Snurr, Nat. Chem. 4 (2011) 83–89.
[9] A.R. Millward, O.M. Yaghi, J. Am. Chem. Soc. 127 (2005) 17998–17999.
[10] A.O. Yazaydın, A.I. Benin, S.A. Faheem, P. Jakubczak, J.J. Low, R.R. Willis, R.Q. Snurr, Chem. Mater. 21 (2009) 1425–1430.
[11] Y. Bae, R.Q. Snurr, Angew. Chem. Int. Ed. 50 (2011) 11586–11596.
[12] E. Haldoupis, S. Nair, D.S. Sholl, J. Am. Chem. Soc. 134 (2012) 4313–4323.
[13] S. Choi, T. Watanabe, T. Bae, D.S. Sholl, C.W. Jones, J. Phys. Chem. Lett. 3 (2012) 1136–1141.
[14] Y. Dai, J.R. Johnson, O. Karvan, D.S. Sholl, W.J. Koros, J. Mem. Sci. 401 (2012) 76–82.
[15] S. Keskin, D.S. Sholl, Langmuir 25 (2009) 11786–11795.
[16] T. Watanabe, D.S. Sholl, Langmuir 28 (2012) 14114–14128.
[17] J.J. Low, A.I. Benin, P. Jakubczak, J.F. Abrahamian, S.A. Faheem, R.R. Willis, J. Am. Chem. Soc. 131 (2009) 15834.
[18] Z. Liang, M. Marshall, A.L. Chaffee, Energy Fuels 23 (2009) 2785–2789.
[19] S. Han, Y. Huang, T. Watanabe, Y. Dai, K.S. Walton, S. Nair, D.S. Sholl, J.C. Meredith, ACS Comb. Sci. 14 (2012) 263–267.
[20] P.M. Schoenecker, H.J. Jasuja, C.G. Carson, C.J. Flemming, K.S. Walton, Ind. Eng. Chem. Res. 51 (2012) 6513–6519.
[21] K. Yu, K. Kiesling, J.R. Schmidt, J. Phys. Chem. C 116 (2012) 20480–20488.
[22] J. Liu, A.I. Benin, A.M.B. Furtado, P. Jakubczak, R.R. Willis, M.D. LeVan, Langmuir 27 (2011) 11451–11456.
[23] N. Audebrand, E. Jeanneau, T. Bataille, S. Raite, D. Louër, Sol. State Sci. 6 (2004) 579–591.
[24] P. Ayyappan, O.R. Evans, W. Lin, Inorg. Chem. 40 (2001) 4627–4632.
[25] G. Peng, Y. Qiu, Z. Liu, Y. Li, B. Liu, H. Deng, Inorg. Chem. Commun. 11 (2008) 1409–1411.
[26] Y. He, J. Li, P. Zhang, X. Chena, Y. Ma, Z. Han, J. Coord. Chem. 61 (2008) 2876–2883.
[27] H. Chun, D.N. Dybtsev, H. Kim, K. Kim, Chem. Eur. J. 11 (2005) 3521–3529.
[28] J. Li, L. Li, J. Liang, P. Chen, J. Yu, Y. Xu, R. Xu, Cryst. Growth Des. 8 (2008) 2318–2323.
[29] L. Pan, M.B. Sander, X. Huang, J. Li, M. Smith, E. Bittner, B. Bockrath, J.K. Johnson, J. Am. Chem. Soc. 126 (2004) 1308–1309.
[30] E. Haldoupis, S. Nair, D.S. Sholl, J. Am. Chem. Soc. 132 (2010) 7528–7539.
[31] S. Keskin, D.S. Sholl, Ind. Eng. Chem. Res. 48 (2009) 914–922.
[32] L. Liu, Q.-F. Deng, Z.-Y. Yuan, J. Mater. Chem. 22 (2012) 15540–15548.
[33] Y.-M. Jeon, G.S. Armatas, J. Heo, M.G. Kanatzidis, C.A. Mirkin, Adv. Mater. 20 (2008) 2105–2110.
[34] Y. Hashimoto, S. Tanaka, Environ. Sci. Technol. 14 (1980) 413.
[35] D.M. Ruthven, Principles of Adsorption and Adsorption Processes, Wiley-Interscience, New York, 1984.
[36] G.J. McManus, Z. Wang, D.A. Beauchamp, M.J. Zaworotko, Chem. Commun. 48 (2007) 5212–5213.
[37] A.I. Skoulidas, D.S. Sholl, J. Phys. Chem. B 106 (2002) 5058–5067.
[38] E. Haldoupis, T. Watanabe, S. Nair, D.S. Sholl, ChemPhysChem 13 (2012) 3449–3452.